Three-dimensional photonic crystal flat lens by full 3D negative refraction

Zhaolin Lu, Shouyuan Shi, Christopher A. Schuetz, Janusz A. Murakowski, and Dennis W. Prather

Department of Electrical and Computer Engineering, University of Delaware, Newark, DE 19716,USA
luzlin@eecis.udel.edu

http://www.eecis.udel.edu/~luzlin/

Abstract: We present the experimental demonstration of imaging by all-angle negative refraction in a 3D photonic crystal flat lens at microwave frequencies. The flat lens is made of a body-centered cubic photonic crystal (PhC) whose dispersion at the third band results in group velocity opposite to phase velocity for electromagnetic waves. We fabricated the photonic crystal following a layer-by-layer process. A microwave imaging system was established based on a vector network analyzer, where two dipoles work as the source and the detector separately. By scanning the volume around the lens with the detector dipole, we captured the image of the dipole source in both amplitude and phase. The image of two incoherent sources separated by 0.44λ showed two resolvable spots, which served to verify sub-wavelength resolution.

OCIS codes: (999.9999) Negative refraction, (999.9999) Photonic Crystal, (999.9999) Flat lens, (100.6640) Super resolution, (220.3620) Lens design, (110.6880) Three-dimensional image acquisition, (110.2990) Image formation theory, (120.5050) Phase measurement.

References and links

1. V.G. Veselago, "The electrodynamics of substances with simultaneously negative values of permittivity and permeability," Sov. Phys. Usp. **10**,509(1968).
2. J.B. Pendry, A.J. Holden, W.J. Stewart, I. Youngs, "Extremely low frequency plasmons in metallic mesostructures," Phys. Rev. Lett. **76,** 4773–4776 (1996).
3. J.B. Pendry, A.J. Holden, D.J. Robbins, W.J. Stewart, "Magnetism from conductors and enhanced nonlinear phenomena," IEEE Trans. Microw. Theory Techniques **47,** 2075–2084 (1999).
4. D.R. Smith, W.J. Padilla, D.C. Vier, S.C. Nemat-Nasser, S. Schultz, "Composite medium with simultaneously negative permeability and permittivity," Phys. Rev. Lett. **84**, 4184 (2000).
5. R.A. Shelby, D.R. Smith, S. Schultz, "Experimental verification of a negative index of refraction," Science **292**, 77-79 (2001).
6. R.A. Shelby, D.R. Smith, S.C. Nemat-Nasser, S. Schultz, "Microwave transmission through a two-dimensional, isotropic, left-handed metamaterial," Appl. Phys. Lett. **78**, 489 (2001).
7. M. Notomi, "Theory of light propagation in strongly modulated photonic crystals: refractionlike behavior in the vicinity of the photonic band gap," Phys. Rev. B **62,** 10696-10705 (2000).
8. M. Notomi, "Negative refraction in photonic crystals," Opt. Quantum Electron. **34**, 133-143 (2002).
9. H. Kosaka, T. Kawashima, A. Tomita, M. Notomi, T. Tamamura, T. Sato, S. Kawakami, "Superprism phenomena in photonic crystals," Phys. Rev. B **58**, R10096-10099 (2000).
10. J.B. Pendry, "Negative refraction makes a perfect lens," Phys. Rev. Lett. **85**, 3966-3969 (2000).
11. P.V. Parimi, W.T. Lu, P. Vodo, J. Sokoloff, J.S. Derov, S. Sridhar, "Negative refraction and left-handed electromagnetism in microwave photonic crystals," Phys. Rev. Lett. **92**, 127401(4) (2004).
12. E. Cubukcu, K. Aydin, E. Ozbay, S. Foteinopoulou, C.M. Soukoulis, "Electromagnetic wave: negative refraction by photonic crystals," Nature **423**, 604-605 (2003).
13. P.V. Parimi, W.T. Lu, P. Vodo, S. Sridhar, "Photonic crystals: imaging by flat lens using negative refraction," Nature **426**, 404 (2003).
14. Z. Lu, S. Shi, C.A. Schuetz, D.W. Prather, "Experimental demonstration of negative refraction imaging in both amplitude and phase," Opt. Express, **13,** 2007-2012 (2005), http://www.opticsexpress.org/abstract.cfm?URI =OPEX-13-6-2007

#7169 - $15.00 US Received 15 April 2005; revised 19 May 2005; accepted 20 May 2005

15. Z. Lu, C. Chen, C.A. Schuetz, S. Shi, J.A. Murakowski, G.J. Schneider, D.W. Prather, "Subwavelength imaging at microwave frequencies by a flat cylindrical lens using optimized negative refraction," Submitted to Appl. Phys. Lett.
16. C. Luo, S.G. Johson, J.D. Joannopoulos, and J.B. Pendry, "All-angle negative refraction in a three-dimensionally periodic photonic crystal," Appl. Phys. Lett. **81**, 2352-2354 (2002).
17. X. Ao, and S. He, "Three-dimensional photonic crystal of negative refraction achieved by interference lithography," Opt. Lett. **29**, 2542-2544(2004).
18. Z. Lu, J.A. Murakowski, S. Shi, C.A. Schuetz, G. J. Schneider, and D.W. Prather, "Three-dimensional subwavelength imaging by a photonic-crystal flat lens using negative refraction at microwave frequencies," Submitted to Phys. Rev. Lett.
19. S. G. Johnson, and J.D. Joannopoulos, "Block-iterative frequency-dormain methods for Maxwell's equations in a planewave basis," Opt. Express **8**, 173-190(2001), http://www.opticsexpress.org/abstract.cfm?URI=OPEX-8-3-173
20. K.M. Ho, C.T. Chan, and C.M. Soukoulis, "Existence of a photonic gap in periodic dielectric structure," Phys. Rev. Lett. **65**, 3152 (1990).
21. J.W. Goodman, *Introduction to Fourier Optics*, pp57-58, McGraw-Hill Companies, Inc. 1996.
22. V.A. Podolskiy, and E.E. Narimanov, "Near-sight superlens," Opt. Lett. **30**, 75(2005).

1. Introduction

Naturally occurring bulk materials typically obey Snell's law with positive refractive indices. However, it has been shown recently that some artificially prepared metamaterials [1-6] and photonic crystals (PhCs)[7-9] exhibit negative refraction. New materials with negative refractive index are rewriting the laws of optics and may allow for the realization of a lens having flat surfaces, no optical axis, and a resolution independent of working wavelength [10]. Along these lines, experiments have demonstrated negative refraction [11,12], and negative refraction imaging by 2D PhC flat lenses [13-15]. However, these 2D flat lenses have shown lensing ability only along one direction, which corresponds to conventional planar lenses [13] or cylindrical lenses [14,15] and, consequently, have limitations for realistic applications. Strictly speaking, they are not fully functional lenses yet. Instead, most applications require the use of spherical lenses. For this reason, "flat spherical" lenses, which work by full 3D negative refraction (F3DNR) and provide super resolution imaging, are especially desired. The realization of such lenses is not only important for many applications, but also significant for fundamental research since F3DNR is a basic physical phenomenon that until now has never been experimentally demonstrated. Thus, the ultimate solution is to demonstrate a lens providing super resolution images based on full 3D negative refraction (F3DNR), which, fortunately, has been investigated theoretically and numerically [16,17]. However, experimental demonstration of such lenses has never been reported since the fabrication of 3D PhCs is difficult, and engineering PhCs with such anomalous dispersion, F3DNR, is even more challenging. In the present work, we have overcome these challenges and succeeded in fabricating such a lens.

2. Three-dimensional photonic crystal with F3DNR

Following a layer-by-layer process and using a CNC micro-milling machine, we fabricated the body-centered cubic (bcc) structure proposed by Luo, *et al* [16] in a low loss dielectric material with ε_r=25 at microwave frequencies. It has a conventional unit cell as shown in Fig. 1(a). There is one air cube at each corner and at the center of a conventional cubic cell. Figure 1(b) shows the bcc structure we fabricated. It is composed of 20 layers, and each layer has a thickness of 6.35mm. The details of the fabrication process were presented in [18].

Using the plane-wave expansion method in Maxwell's equations, we solved for the eigen-frequencies for a given wave vector [19,20]. Figure 1(c) shows the dispersion diagram of the bcc photonic crystal, which is very similar to that presented by Luo *et al* [16]. The top of the third band is simple and curved downwards, which makes full 3D negative refraction possible. For electromagnetic waves with frequencies at the top range of the third band, it is likely to hold isotropic dispersion. However, compared with their results, for the first three bands each of the corresponding frequency scale in our dispersion diagram is compressed to nearly 88% due to the change of dielectric constant from ε_r=18 to ε_r =25. As a result, F3DNR is expected

#7169 - $15.00 US Received 15 April 2005; revised 19 May 2005; accepted 20 May 2005

to occur at (0.33, 0.36) c/a, or (15.6GHz, 17.0GHz). In particular, n_{eff}=-1 (with variation of 3%) is found at f=17.0GHz.

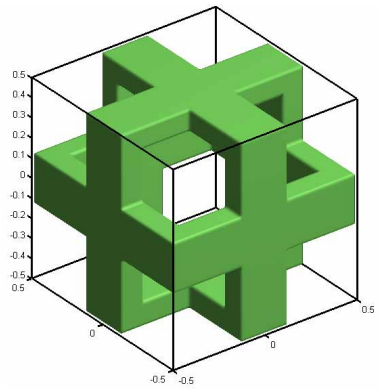

(a)

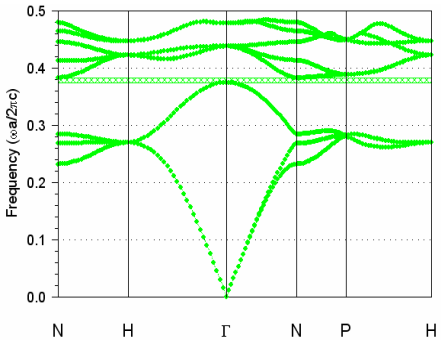

(c)

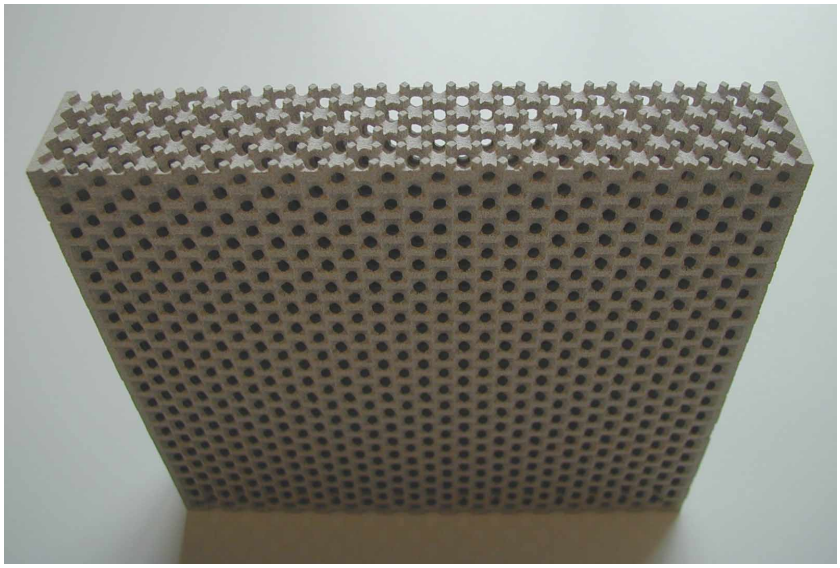

(b)

Fig. 1. (a) Conventional cubic cell of the bcc structure. (b) Three-dimensional PhC fabricated layer-by-layer (20 layers in total). Note that (101) plane works as the flat lens surface, so the lattice orientation has rotated 45º surrounding vertical axis. (c) Band structure of the bcc lattice photonic crystal.

3. Experiments

To test the performance of the lens, we built a microwave imaging setup based on an Agilent 85106D vector network analyzer. Two dipoles were placed along x-axis, working as the source and the detector, separately. (In the description, we use Cartesian coordinates with origin in the middle of the lens surface on the image side. z-axis coincides the optical axis, whereas x-axis and y-axis represent the horizontal and vertical directions, respectively. See

#7169 - $15.00 US
Received 15 April 2005; revised 19 May 2005; accepted 20 May 2005

also inset in Fig.4 (a). The detector is mounted on an XYZ scanner to map the electric field. The field distribution is acquired by scanning the object space and image space.

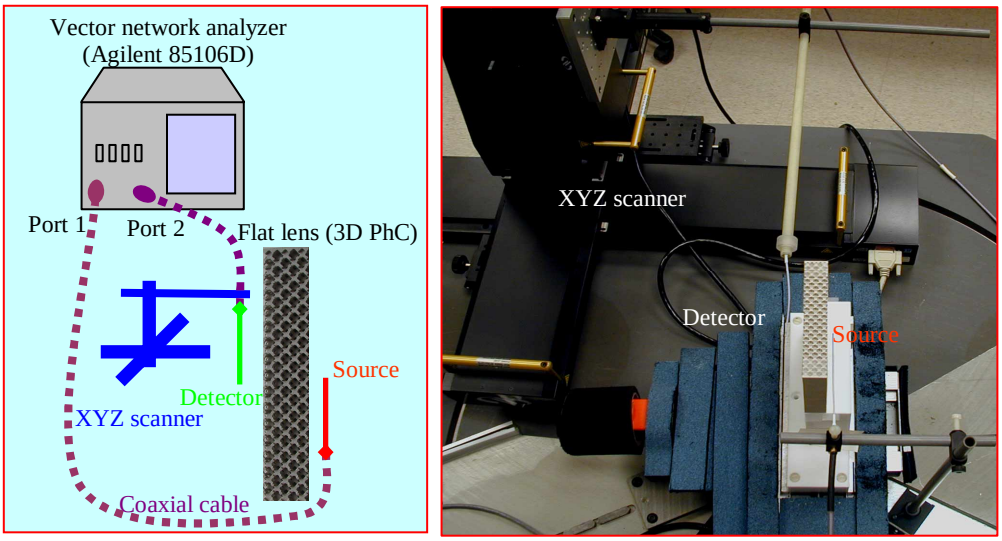

Fig. 2. Experimental setup for acquiring three-dimensional field distribution.

A custom program was developed to synchronize the scanning and measurement. Once a scanning and measurement is finished, we depict the S-parameter value, S_{21} in our case, with regard to the position as an image. Consequently, each pixel in the image corresponds to the S-parameter value at a scanning position. In addition, in the network analyzer the S-parameters are given as complex values, so we obtain both amplitude and phase distributions, which is difficult for near infrared or visible light measurement.

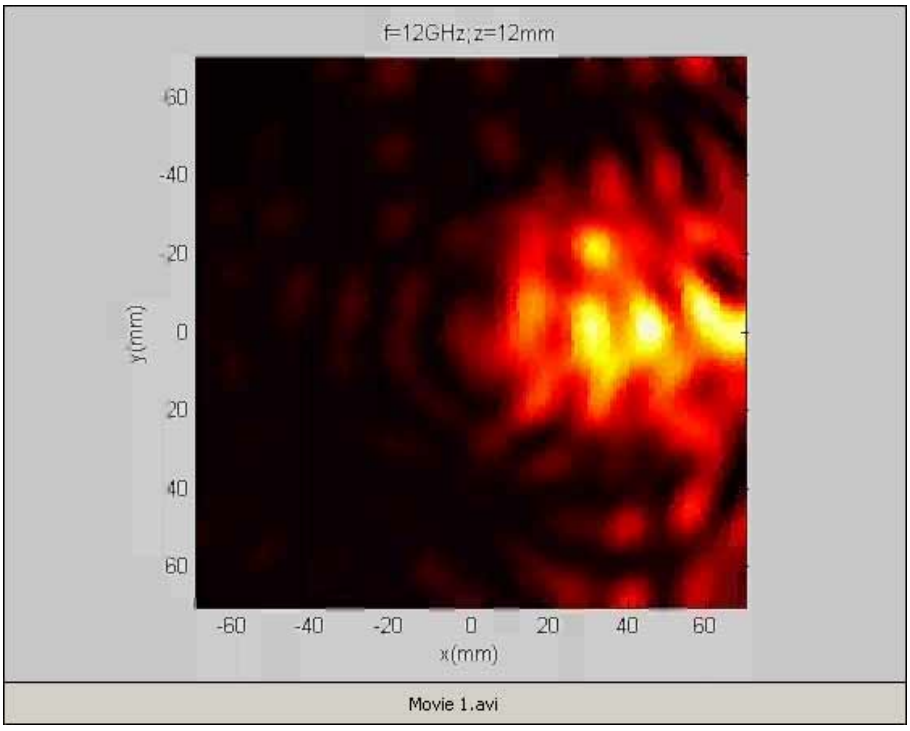

Fig. 3. Amplitude distributions changing with the frequency (multimedia movie, 392KB).

#7169 - $15.00 US
Received 15 April 2005; revised 19 May 2005; accepted 20 May 2005

The PhC flat lens is placed on a Teflon bar, which has low dielectric constant, and the source dipole is placed at the center, 3mm away from the lens surface on the object side, i.e, object distance d_o=3mm. Due to the difference between the mathematical model and the actual situation, it is often difficult to accurately predict where the image is located and exactly for which frequency range F3DNR occurs. Therefore, we approached and explored the image in a step-by-step fashion.

First, we scanned the image field distribution with step size (or pixel) of 1mm×1mm in the vertical or *xoy* plane, just outside the lens on its image side (z=2mm). Meanwhile we spanned the frequency from 12.0GHz to 20.0GHz with a spacing of 0.2GHz. For each frequency, we *mathematically* reconstructed the field distribution along z-axis based on the corresponding *measured* amplitude and phase distributions at the z=2mm plane [21]. The result of this process was the location of good images at z=12mm in the frequency range 16.0GHz~17.2GHz. Based on this result, we moved the detector to z=12mm and repeated the measurement in the vertical plane *xoy*. The measured results confirmed that good images were indeed observed in the frequency range 16.0GHz~17.2GHz. Figure 3 (multimedia movie) shows how the *measured* amplitude distribution changes with the frequency.

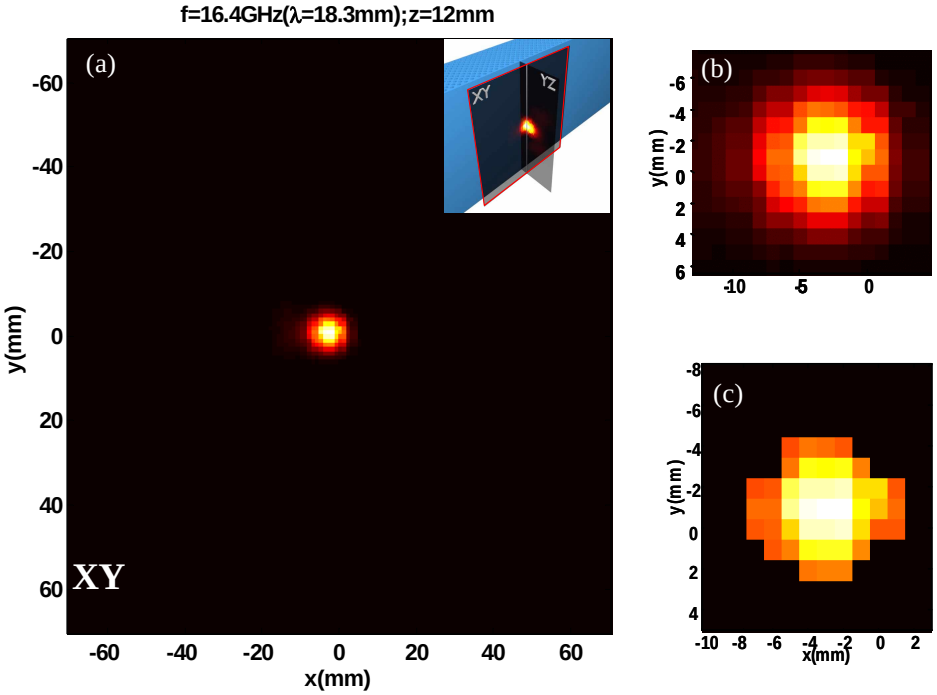

Fig. 4. Image of a microwave dipole achieved through the 3D PhC flat lens at image distance, d_i=12mm. (b)(c). The image size full width at half maximum (FWHM) is found to be 9mm×7mm. The working frequency is f=16.4GHz (λ=18.3mm).

Once the frequency range and image position are experimentally determined, we performed a dense scan in the frequency range 15.5GHz~17.5GHz with spacing 0.1GHz. Figure 4 shows the image (intensity) obtained at f=16.4GHz (λ=18.3mm). According to this intensity distribution, the image size is calculated to be 9mm×7mm using full width at half maximum (FWHM) criterion, which represents only 44% of the vacuum wavelength. Therefore, the experiment successfully validates sub-wavelength feature size produced by the 3D PhC flat lens. The refractive index at 16.4GHz is theoretically calculated to be n_{eff}=–1.05

#7169 - $15.00 US
Received 15 April 2005; revised 19 May 2005; accepted 20 May 2005

when the photonic crystal is treated as an infinitely periodic structure. However, according to our measurements the object distance (3mm) plus image distance (12mm) is considerably smaller than the lens thickness (25mm). So, the image distance is smaller than the expected value.

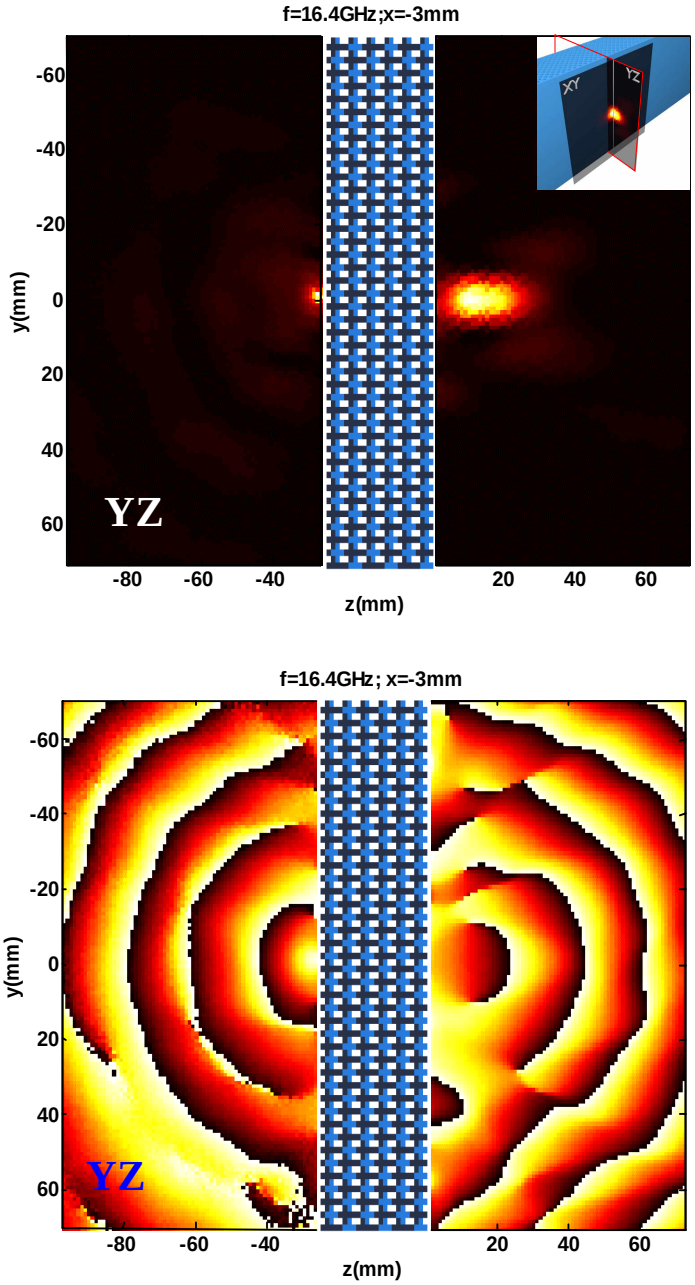

Fig. 5. (a) Measured amplitude distribution. The amplitude scale on the source side varies from -41 dB (yellow) to -80 dB (black), and on the image side from -49 dB to -80 dB. (b) Phase distribution in vertical plane.

#7169 - $15.00 US
Received 15 April 2005; revised 19 May 2005; accepted 20 May 2005

To see the image formation more clearly, we also scanned the image space along vertical plane *yoz* and horizontal plane *xoz*. In addition, we repeated the measurements on the corresponding planes in object space. To fully show the image formation, we put the field distribution of the object and that of the corresponding image on the same figure. Figure 5 shows the amplitude and phase distributions along vertical plane. In the figure, the side view of the PhC lens is depicted between the object and image. The high amplitude spot along with the closed phase circle in the vertical plane indicates how the image is formed. In the horizontal plane, similar result was obtained.

In addition, we scanned a full 3D field distribution in the image space point by point with pixel size 2mm×2mm×2mm, and the total volume 140mm×140mm×50mm. The frequency range spanned from 15.5GHz to 17.5GHz with spacing 0.1GHz. In this way, we were able to obtain 3D images of the dipole source shown in both amplitude and phase. We found the best 3D images in the 16.0GHz~17.2GHz range. As an example, Fig. 6 (multimedia movie) shows the amplitude changing along *z*-axis for 16.4GHz. It is seen that the electromagnetic waves converge first, and then diverge into far field, which precludes the possibility that the sub-wavelength image is observed because the detector is very close to the source (object).

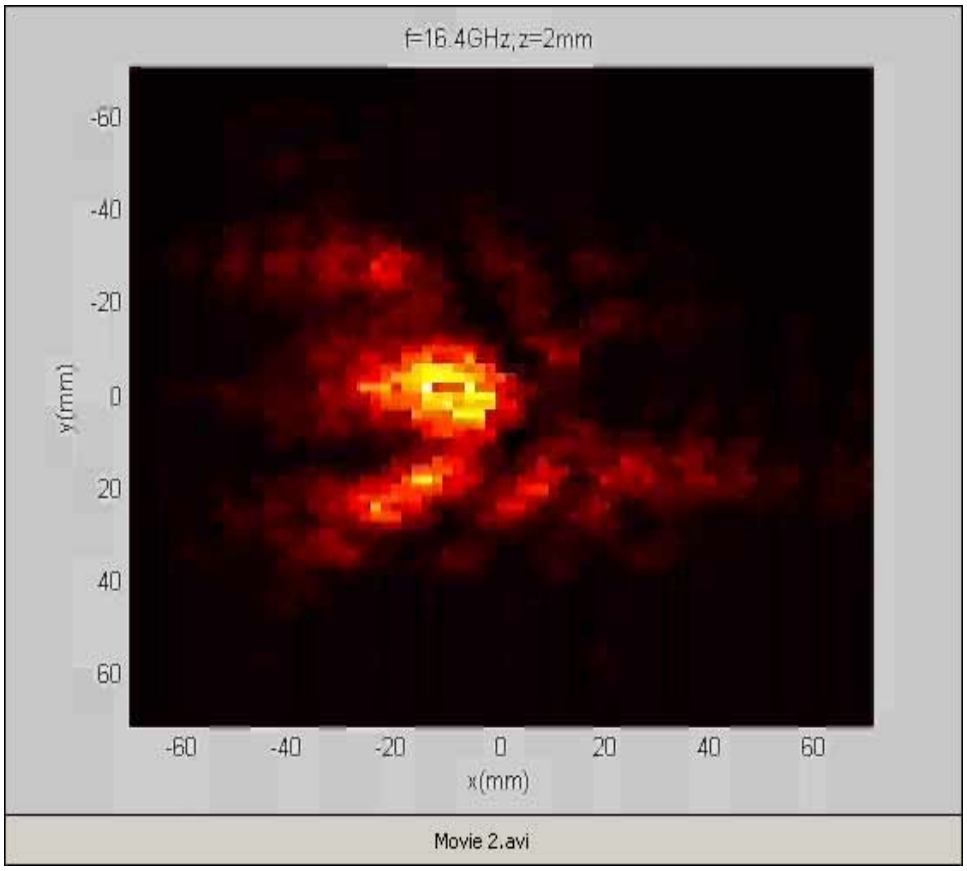

Fig. 6. The amplitude changing along z-axis for 16.4GHz (multimedia movie, 392KB).

To further validate the sub-wavelength resolution, we employed two x-polarized dipole sources from two different vector network analyzers with d_o=3mm and aligned the sources on y-axis, 8mm (0.44λ, λ=18.3mm) apart. We balanced the powers of the sources and repeated the scanning in the vertical plane at z=12mm. During the scanning, we alternately used the network analyzers to measure the field at each position. Figure 7(a) shows the image we

#7169 - $15.00 US Received 15 April 2005; revised 19 May 2005; accepted 20 May 2005

obtained at that plane. Shown in Fig. 7(b) is a line scan taken along the white line in Fig.7(a), where clearly visible are two peaks 8mm apart; this corresponds to separation of only 0.44λ! This result, combined with the result shown in Fig. 4 confirms that sub-wavelength imaging is achieved for an object containing sub-wavelength feature size. Thus, the lens is capable of sub-wavelength imaging from both viewpoints of the object and of the image. For comparison, a conventional lens forms image at far field, where the resolution is restricted by the diffraction limit to half wavelength [22]. In contrast, our flat lens works by amplifying evanescent waves, forms images at near field (image distance=0.66 λ, λ=18.3mm), and overcomes the diffraction limit. In this sense, our imaging system exhibits super-resolution and our lens is a superlens.

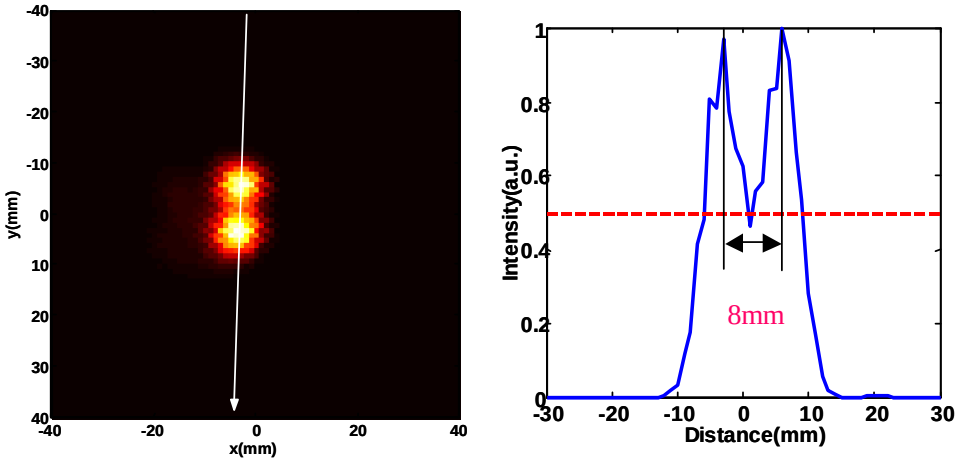

Fig. 7. (a) The image (intensity) of two sources from two different vector network analyzers. (b) The intensity distribution along the white line marked on (a). The image shows two resolvable spots with distance 8mm (0.44λ, λ=18.3mm).

4. Conclusions

In conclusion, we fabricated and characterized a 3D bcc lattice PhC flat lens. We performed a series of experiments on this lens that demonstrated and explored F3DNR imaging of a point source in both amplitude and phase. The analysis of the acquired field distribution demonstrated sub-wavelength imaging using F3DNR! We introduced a two-source configuration and validated sub-wavelength (0.44λ) resolution. In addition, the resolution is better than diffraction limit, which proves that the lens overcomes the diffraction limit and allows for super-resolution imaging. These results have both theoretical and experimental significance.

#7169 - $15.00 US Received 15 April 2005; revised 19 May 2005; accepted 20 May 2005